The Journal of Chemical Physics

Relating free energy and open-circuit voltage to disorder in organic photovoltaic systems

Cite as: J. Chem. Phys. **149**, 244123 (2018); https://doi.org/10.1063/1.5050506
Submitted: 31 July 2018 . Accepted: 19 November 2018 . Published Online: 31 December 2018

V. Lankevich, and E. R. Bittner

Relating free energy and open-circuit voltage to disorder in organic photovoltaic systems

V. Lankevich[a] and E. R. Bittner[a,b]
Department of Chemistry, University of Houston, Houston, Texas 77204-5003, USA

(Received 31 July 2018; accepted 19 November 2018; published online 31 December 2018)

Efficient exciton dissociation into mobile charge carries a crucial factor underscoring the performance of organic polymer-based bulk-heterojunction photovoltaic devices. In this paper, we compute the energies of charge-transfer (CT) states of the model donor-acceptor lattice system with varying degrees of structural disorder to investigate how fluctuations in the material properties affect electron-hole separation. We also demonstrate how proper statistical treatment of the CT energies recovers the experimentally observed "hot" and "cold" exciton dissociation pathways. Using a quantum mechanical model for a model heterojunction interface, we recover experimental values for the open-circuit voltage at 50 and 100 meV of site-energy disorder. We find that energetic and conformational disorder generally facilitates charge transfer; however, due to excess energy supplied by photoexcitation, highly energetic electron-hole pairs can dissociate in unfavorable directions, potentially never contributing to the photocurrent while "cold" excitons follow the free energy curve defined at the operating temperature of the device. *Published by AIP Publishing.* https://doi.org/10.1063/1.5050506

I. INTRODUCTION

Abundance of sunlight on the surface of the earth strongly favors solar cells as the replacement of fossil fuels as a primary energy resource. We are particularly interested in organic photovoltaic devices (OPVs) that have attracted considerable attention due to their promising electronic properties, cost effectiveness, and customizability.[1–4] However, the lack of complete understanding of physical processes that guide current generation in morphologically complex OPVs has stymied their full potential on a commercial scale. Figure 1 outlines the elementary steps of energy transfer and charge generation following photo-excitation in a donor-acceptor system.

Successful dissociation of electron-hole pairs separated by the donor-acceptor boundary [charge-transfer (CT) states] into free charge carriers is especially puzzling since it requires an electron and a hole to overcome the strong electrostatic attraction under seemingly unfavorable conditions. More specifically, we consider an electron *free* when the strength of the Coulombic interaction that binds it to the hole is comparable with thermal fluctuations of the material. This condition can be expressed in the following way:

$$\frac{e^2}{4\pi\epsilon_0\epsilon r} \leq k_B T, \tag{1}$$

where e is the electron charge, ϵ_0 is vacuum permittivity, ϵ is the dielectric constant of the material, and r is the distance between an electron and a hole. Due to the low dielectric constant (ϵ = 2–4) of organic materials typically used in OPVs, an electron finds itself with a 0.5 eV barrier to surmount, corresponding to the Coulomb capture radius of 15–28 nm. It is highly improbable that charges would be able to move this distance before recombining; however, it has been observed that free charge carriers can be formed at separations of 4 nm on the femtosecond time scales.[5,6]

The apparent disparity between the simple energetic estimate and the experimental evidence stems from the neglect of entropic effects in the estimate provided by Eq. (1). Durrant and Clarke have pointed out that an electron can take various possible paths to decouple from the hole and reach the free carrier state.[7] The electron-hole density of states depends not only on the energy of the pair but also on the magnitude of charge separation because the farther an electron and a hole travel from each other, the greater is the number of possible dissociation paths that can be taken to achieve a given separation. Consequently, energetic considerations alone do not offer a complete picture of the charge dissociation, and to gain a better understanding of the process, one should compute the (Helmholtz) free energy as a function of electron/hole separation distance, r,

$$F(r) = U(r) - TS(r) = U(r) - k_{BT} \ln \Omega(r), \tag{2}$$

where $\Omega(r)$ is the number of equivalent electron/hole states with separation r, T is the absolute temperature, k_B is the Boltzmann constant, $U(r)$ is the electron-hole interaction potential, and S is the entropy of the electronic degrees of freedom.

In an ordered material, dimensionality is a key factor that determines the relevance of the entropy term. Gregg argues that a π-electron confined to move along a single quasi-one-dimensional polymer chain has only one defined path and consequently the electronic entropy is exactly zero. Moreover, for thin-films (2-D) and fullerene-based acceptors (3-D), the

[a]URL: http://k2.chem.uh.edu/.
[b]Electronic mail: ebittner@central.uh.edu

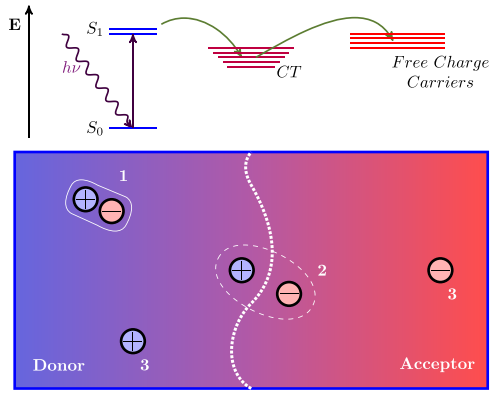

FIG. 1. Schematic diagram of exciton dissociation and formation of free charges in bulk-heterojunction OPVs. Photoexcitation produces an exciton (1) in the donor, the acceptor or at the interface between them. Excitons created in the donor phase diffuse toward the interface (2) where energetic offset forces them to dissociate and separate apart, ideally, becoming free charges (3).

number of electron/hole configurations available to the system with a given electron/hole separation radius scales with the surface area

$$\Omega \propto (r/r_o)^{d-1}, \tag{3}$$

where r_o is the unit length and d is the dimensionality of the system. Consequently, the entropy,

$$S = (d-1)\ln(r/r_o),$$

can become energetically comparable to the Coulombic energy of the electron-hole pair in two and three dimensions.[8,9] This estimate, however, is only valid for the scenarios with an immobile hole. Allowing the hole to move adds additional degrees of freedom and increases the number of available electronic states further emphasizing the importance of entropic contribution.

Generally speaking, organic semiconductors are disordered and amorphous systems. Besides dimensionality, the free energy needs to reflect a non-uniform landscape of donor and acceptor energies, as well as the finite lifetime of the CT state that can eliminate a sizable fraction of the possible dissociation routes.[8]

Entropy and free energy are state functions, and to employ them, we need to be certain that the system we are studying is in equilibrium. Burke *et al.* argue that this is the case for organic photo-excited materials since post-dissociation electron-hole encounters do not result in an immediate recombination. Instead, electrons and holes meet and separate several times before, eventually, recombining. A faster rate of separation leads to a rapid equilibrium between interfacial charge-transfer states and free carrier species. This equilibrium condition then implies an equality between the chemical potential and the open-circuit voltage, qV_{OC}, of the photo-voltaic device.[10]

This equality, therefore, establishes a crucial connection between theoretical and laboratory investigations of the current generation in OPVs. Burke and colleagues arrive at the following expression for the V_{OC} from the canonical ensemble:

$$qV_{OC} = E_{CT} - \frac{\sigma_{CT}^2}{2kT} - kT\log\left(\frac{qfN_0L}{\tau_{CT}J_{sc}}\right), \tag{4}$$

where f is the volume fraction of the device that is mixed or interfacial, L is the thickness of the solar cell, J_{SC} is the short-circuit current of the cell, q is the electric charge, and N_0 is the density of the electronic states in the device. Most importantly, Eq. (4) includes the necessary dependence of qV_{OC}, and therefore of F, on the average energy of the CT state, E_{CT}, and disorder in the CT energies, expressed through standard deviation, σ_{CT}, and the lifetime of the CT-state, τ_{CT}.[10] Nonetheless, this expression is composed of variables that refer to the entire device making Eq. (4) computationally inapplicable.

Following Clarke and Gregg's work, Hood and Kassal have shown that the change in the free energy better reflects the energy landscape that an electron and a hole traverse because entropic considerations lower the energy barrier needed for an electron to become a free charge carrier. Additional dissociation paths and energetic disorder make the Coulombic interaction comparable to thermal fluctuations, so it no longer defines how far an electron and a hole can separate. Hood and Kassal model a bulk-heterojunction as an ensemble of energetically disordered hexagonal lattices and compute the electronic density of states as a function of the electron-hole separation for each. Under the assumption of electronic equilibrium, authors then compute the entropy and the free energy in the following way:[9]

$$F = -\langle k_BT\ln Z\rangle \tag{5}$$

where Z is the partition function that describes specific energy states and the bracket $\langle\cdots\rangle$ denotes a statistical average over realizations of the disordered lattice. Both Eqs. (4) and (5) are derived in the canonical ensemble and carry the same information. However, the latter approach is far more suitable for connecting to microscopic details such as energetic and structural disorder.

There are, however, a few drawbacks of the Hood-Kassal model. The electrons and holes are not permitted to cross from one domain to the other, and a hole is restricted to move only perpendicular to the interface under the assumption of translational symmetry. The model includes the electrostatic potential, but does not take into account important quantum effects such as delocalization, mixing between excitonic and charge-transfer configurations, and electronic exchange effects.

In this work, we use a fully quantum mechanical model of the electronic states of a bulk-heterojunction interface to investigate how the presence of disorder in OPVs influences the free energy of an electron as it separates away from the interface into the free carrier phase, taking into account Coulombic and exchange interactions, lattice vibrations, and electron-phonon couplings. In addition, we examine the role of bandwidth and interfacial driving forces in determining the dissociation free energy of an electron/hole pair. Our model combines quantum and statistical treatments of a system with the large number of parameters and all possible electron-hole configurations

to give results that provide a unifying picture linking various proposed mechanisms for charge separation.

II. METHODS

A. Model Hamiltonian

The region of donor-acceptor interface of an OPV is generalized to the square lattice system, where each site is characterized by a valence energy and a conduction band energy coupled to two phonon modes associated with lattice vibrations. We have used this model extensively to study photo-induced processes in organic polymer semiconductors.[11–17] The model is described by the following system-plus-bath Hamiltonian:[18,19]

$$\begin{aligned}\hat{H} &= \hat{H}_{el} + \hat{H}_{el-ph} + \hat{H}_{ph} \\ &= \sum_{\mathbf{mn}} (F_{\mathbf{mn}} + V_{\mathbf{mn}}) |\mathbf{m}\rangle\langle\mathbf{n}| + \sum_{\mathbf{mn},a,\mu} \Big(\frac{\partial F_{\mathbf{mn}}}{\partial q_{a,\mu}}\Big) q_{a,\mu} |\mathbf{m}\rangle\langle\mathbf{n}| \\ &\quad + \frac{1}{2} \sum_{\mu,a} \omega_a^2 (q_{a,\mu}^2 + \lambda q_{a,\mu,\mu+1}) + p_{a,\mu}^2, \end{aligned} \tag{6}$$

where electron-hole configurations $|\mathbf{n}\rangle = |\mathbf{h}_i\mathbf{e}_j\rangle$ whereby a hole in a valence orbital on site i and an electron in a conduction orbital on site j form the basis for the Hamiltonian. We have published the details and parameterization of the model previously and, we briefly review its salient features. The term $F_{\mathbf{mn}}$ describes the single-particle motion for a non-interacting electron/hole pair. In its simplest form for configurations $|\mathbf{n}\rangle = |\mathbf{h}_i\mathbf{e}_j\rangle$ and $|\mathbf{m}\rangle = |\mathbf{h}_k\mathbf{e}_l\rangle$, it is given by

$$F_{\mathbf{mn}} = f^e_{jl}\,\delta_{ik} + f^h_{ik}\,\delta_{jl}, \tag{7}$$

where f^e and f^h have the meaning of localized energy levels and transfer integrals for conduction band electrons and valence band holes. In the absence of disorder, these quantities obey charge-conjugation symmetry with $f^h_{mn} = -f^e_{mn}$ and we assume that only the nearest neighbors on the 2D lattice are coupled by these terms ($f_{i,i+1} = t$). The donor and acceptor domains are differentiated by imposing an energetic off-set, ΔE, in the site-energies at the domain boundary as sketched in Fig. 2. $V_{\mathbf{mn}}$ describes spin-dependent two-particle Coulombic and exchange interactions for each configuration, as well as interactions between different singlet geminate electron-hole pairs. For the case of singlet excitations,

$$V_{\mathbf{mn}} = -\langle h_i e_j|V|h_i e_j\rangle + 2\langle h_j e_i|V|h_i e_j\rangle. \tag{8}$$

We assume that the inter-unit overlap of the primitive site-basis functions is small and that three types of integrals contribute to this interaction, each with well known meaning and long-range behavior.[19] First, an electron and a hole on site separated by a distance r will experience a long-range Coulomb attraction of the Mataga-type

$$\langle h_i e_j|v|h_i e_j\rangle = \frac{J_o}{1 + r_{ij}/r_o}, \tag{9}$$

a short range exchange term which decays exponentially with electron/hole separation

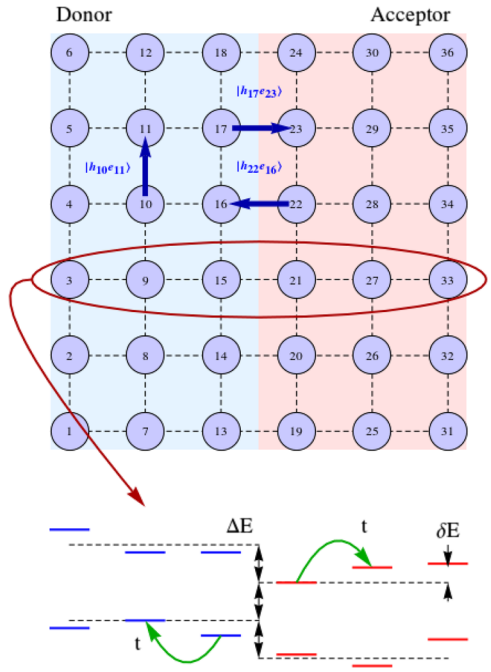

FIG. 2. Schematic representation of the lattice model and conduction and valence band energies associated with each site. Donor and acceptor phases are distinguished by lowering the acceptor site energies by ΔE. t is the hopping parameter controlling electron and hole's movement between the neighboring sites. Disorder is introduced into the model by modifying energy of each site by some value randomly drawn from a Gaussian distribution with variance δE. $|h_{17}e_{23}\rangle$, $|h_{22}e_{16}\rangle$, and $|h_{10}e_{11}\rangle$ are examples of CT, "flipped" CT, and an "intraphase" CT configurations, respectively.

$$\langle h_j e_i|v|h_i e_j\rangle = K_o \exp(-r_{ij}/r_o). \tag{10}$$

Second, because differential overlap between an electron and a hole sitting on the same site is substantial, we include the transition dipole-dipole coupling between singlet geminate electron hole pairs,

$$\langle h_i e_i|v|h_j e_j\rangle = \frac{D_o}{(r_{ij}/r_o)^3}, \tag{11}$$

where J_0 and K_0 indicate Coulombic and exchange interactions between an electron and a hole on the same site. D_0 is a dipole moment of an electron-hole pair located on site i. The parameters for our model are included in the supplementary material. It is important to note that these terms carry information pertaining to the spatial disorder in our model. While the model can treat singlet or triplet states, we are analyzing post-photoexcitation charge-transfer states and will only focus on singlets in this study.

The phonon term, $\hat{H}_{ph}$, assigns to each lattice site a high and a low frequency vibrational mode described by a local harmonic oscillator with weak nearest-neighbor coupling. These terms are determined from spectroscopic Huang-Rhys parameters typifying organic conjugated polymer systems. Such contributions modulate *both* the on-site bandgap as well as the site-to-site hopping integrals.

For a given phonon configuration, the eigenstates of the Hamiltonian in Eq. (6) are linear combinations of all configurations allowed on a particular lattice

$$(\hat{H}_{el} + \hat{H}_{el-ph}(\{\mathbf{q}\}))|\mathbf{\Psi}^k\rangle = \mathbf{E}_k(\{\mathbf{q}\})|\mathbf{\Psi}^k\rangle \tag{12}$$

with the kth eigenstate defined as $|\Psi^k\rangle = \sum_{ij} c_{ij}^k |h_i e_j\rangle$. We construct a 10 site × 10 site lattice with a donor-acceptor energy offset of $\Delta E = 0.5$ eV, the transfer energy between nearest sites set to $t = 0.536$ eV, and lattice constant $a = 1$ nm in all directions. We deliberately choose a higher value for the hopping parameter (previously calculated to represent polymer intrachain transfer energy[18]) to allow an electron and a hole easy passage throughout the lattice and to insure that nothing but the presence of disorder inhibits or facilitates electron/hole dissociation.

Once we obtain eigenvalues of the system Hamiltonian and the corresponding electron-hole separations, we compute average and free energies of the e-h pair as a function of the average electron/hole separation for a given state. This is accomplished by binning each state according to its eigenenergy and the expectation value of r_{eh} as described in Sec. II B. Since the full CI approach for the 10 × 10 lattice results in 10 000 eigenstates for each realization with 90% of the eigenvalues lying well above the range for UV and visible excitation, we impose an energy cutoff of 3.1 eV for our sampling. Furthermore, to avoid issues with the finite lattice size, we consider only e/h separations up to 5 a, where a is the lattice constant as defined above.

B. Eigenstate analysis

In order to analyze the resulting states, we map a configuration with a hole on site i and an electron on site j onto a lattice in the Cartesian plane to compute electron-hole separation $r_{ij} = \sqrt{(x_i - x_j)^2 + (y_i - y_j)^2}$, where (x_i, y_i) and (x_j, y_j) are site-wise coordinates of a hole and an electron, respectively. We define operator $\hat{R}$ such that $\hat{R}|\mathbf{h}_i\mathbf{e}_j\rangle = r_{ij}|\mathbf{h}_i\mathbf{e}_j\rangle$ to compute the expected e-h separation $\langle R\rangle$ for kth eigenstate $|\Psi^k\rangle$ of $\hat{H}_{el} + \hat{H}_{el\text{-}ph}$ and to match it to the corresponding eigenvalue

$$\langle R^k\rangle = \langle\Psi^k|\hat{R}|\Psi^k\rangle = \sum_{ij} |\rho_{ij}^k| r_{ij}, \tag{13}$$

where $|\rho_{ij}^k| = c_{ij}^{*k} c_{ij}^k$ represents a contribution of configuration $|\mathbf{h}_i\mathbf{e}_j\rangle$ to the electron-hole separation of the kth eigenstate $|\Psi^k\rangle$.

Removing any restriction on where on the lattice an electron and a hole can be located gives us a more detailed model of the system but comes at a disadvantage because now in addition to the charge-transfer states defined above, we need to consider "flipped" CT states with holes in the acceptor and electrons in the donor, as well as states with both particles located in the same phase. To clarify the nature of each eigenstate, we also define a dipole operator as $\hat{P}|\mathbf{n}\rangle = \hat{P}|\mathbf{h}_i\mathbf{e}_j\rangle = \mathrm{sgn}(i-j)er_{ij}|\mathbf{h}_i\mathbf{e}_j\rangle$, where e is the elementary charge and $\mathrm{sgn}(i-j)$ ensures that the dipole is correctly defined as pointing from an electron on site e_j to a hole on site h_i

$$\begin{aligned}\langle R_D^k\rangle = \frac{\langle\Psi|\hat{P}|\Psi\rangle}{e} &= \frac{\langle\Psi|\sum_{ij} c_{ij}^k \hat{P}\,|\mathbf{h}_i\mathbf{e}_j\rangle}{e} \\ &= \frac{\sum_{ij}\mathrm{sgn}(i-j)\,|\rho_{ij}^k|\,e\,r_{ij}}{e} \\ &= \sum_{ij}\mathrm{sgn}(i-j)\,|\rho_{ij}^k|\,r_{ij}. \end{aligned}\tag{14}$$

We emphasize the difference between the dipole moment computed in Eq. (14) and the transition dipole moment often calculated in relation to charge-transfer states. The transition dipole moment is the off-diagonal element of the dipole operator $\hat{P}$ and gives the likelihood of the electron transition between two different states $|\Psi^a\rangle$ and $|\Psi^b\rangle$. We are computing the diagonal elements of the said operator which correspond to the electric dipole moment of the charge distribution of the k-th state $|\Psi^k\rangle$. Site localization of an electron and a hole of basis configurations allow us to compute the total electric dipole moment, and therefore the dipole size, of each eigenstate as the sum of dipole moments of classical charged pairs.

Figure 2 illustrates some of the possible configurations of the system to explain the difference between $\langle R\rangle$ and $\langle R_D\rangle$. The configuration $|h_{22}e_{16}\rangle$ will have the same e-h separation as the charge-transfer configuration $|h_{17}e_{23}\rangle$; however, its dipole is reversed since the spatial position of the electron and hole have been swapped. In addition, it is important to realize that for each configuration $|\mathbf{h}_i\mathbf{e}_j\rangle$, there is a configuration $|\mathbf{h}_j\mathbf{e}_i\rangle$; however, $|\rho_{ij}|$ does not have to be equal to $|\rho_{ji}|$. Excitonic configurations such as $|h_ie_i\rangle$ do not contribute to the polarization of the system since the electron and hole reside on the same site, and hence $r_{ii} = 0$. Kets $|h_{17}e_{23}\rangle$, $|h_{22}e_{16}\rangle$, and $|h_{10}e_{11}\rangle$ represent CT, "flipped" CT, and "intraphase" CT configurations, respectively. By examining the relationship between the eigenvalues of $\hat{H}_{el} + \hat{H}_{el\text{-}ph}$ and distances $\langle R\rangle$ or $\langle R_D\rangle$, we can determine what changes in model parameters facilitate formation of free charges.

C. Disorder and energy calculations

To model disorder, we introduce fluctuations into the lattice parameters and create 1000 versions (realizations) of the lattice, each time randomly drawing the values of these parameters from a Gaussian distribution. The variance of the said distribution represents the amount of disorder in the chosen parameter. Our main concern in this work is disorder in the band energies of each site, δE, but we also look into fluctuations in the hopping parameter, δt, and the site position, $(\delta x, \delta y)$. Each realization yields a set of eigenstates of the system. Combined together, eigenstates from all realizations produce more detailed energy-separation and energy-dipole spectra. Figure 3 shows a typical result from our simulations. Energy-dipole and energy separation spectra throught this paper are visualized as non-weighted log-scaled probability distributions, where the contours and colors indicate the density of electronic states at a given energy and with a given electron/hole separation [Fig. 3(a)] or dipole size [Fig. 3(b)] according to the definitions given above.

To compute the average energy, $\widetilde{E}$, as a function of $\langle R\rangle$ or $\langle R_D\rangle$, we divide the distribution into intervals of equal width, δR, and average N_i eigenvalues that fall into the ith interval to obtain $\widetilde{E}(R_i) = \sum_j^{N_i} E_j(R)/N_{ij}$, where R_i is the center of the ith interval. This approach, however, assumes that all of the states are equally probable. Diagonalizing the Hamiltonian returns only the values of all possible energy levels, and it is the operating temperature of the device that determines the probability weight of each state. Therefore, the proper thermodynamic

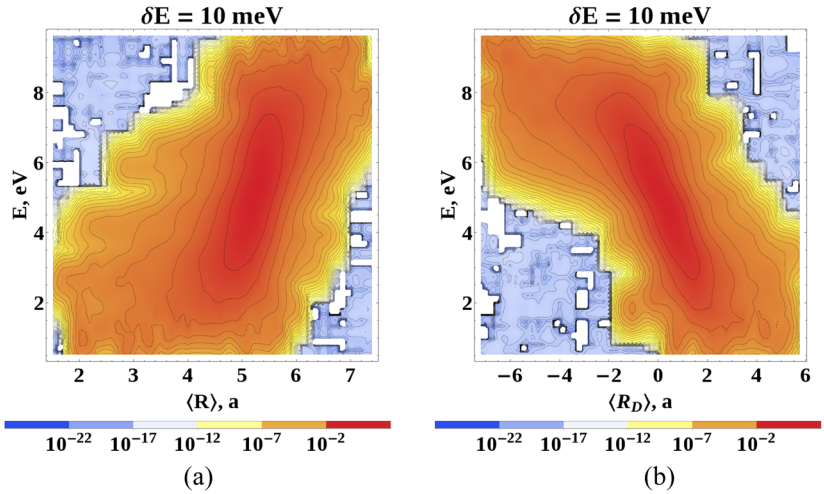

FIG. 3. Probability distributions of CT energies of the system as a function of electron-hole separation, $\langle R \rangle$, and dipole size, $\langle R_D \rangle$. The color map is scaled such with blue and red corresponding to the lowest and highest densities, respectively. The sign of the dipole size depends on the orientation of the CT dipole: if an electron is in the acceptor phase and a hole is in the donor, the dipole size is positive, otherwise it takes on negative values. Distributions are computed for systems with $\delta E = 10$ meV.

energy of the system for a specific *e-h* separation should be computed as follows:[20]

$$\langle E(R_i) \rangle = \frac{\sum_j^{N_i} E_j e^{-\beta E_j}}{\sum_j^{N_i} e^{-\beta E_j}}, \tag{15}$$

where $\beta = 1/k_B T$ and $e^{-\beta E_j}$ is a thermal probability weight of an eigenstate with energy E_j. We compute the free energy on each interval from the partition function to take into the account not only the thermal probability weight of each state, but also the change in entropy of the system due to the presence of disorder

$$F(R) = -kT \ln \Big(\sum_j e^{-\beta E_j(R)} \Big). \tag{16}$$

We incorporate the averaged influence of the vibrational degrees of freedom on the electronic states through the coupling term, $H_{el\text{-}ph}$. As a consequence, without time-dependent nuclear motion, the spatial part of each eigenstate and the geometry of the corresponding charge distribution will not change in time. In order to increase the distance between charges, an electron-hole pair with separation R_i needs to transfer to a state with separation $R_j > R_i$. Connecting the most likely states that can be occupied at each interval, we obtain the expected energy paths. Even though the distribution of CT states is very broad and some *e-h* pairs can potentially dissociate through any other sequence of states, expected energy curves $\widetilde{E}(R)$, $\langle E(R) \rangle$, and $F(R)$ allow us to understand how different parameters of the system influence dissociation of the majority of *e-h* pairs, without investigating numerous individual space-time trajectories. We choose the interval width to be $\delta R = 0.1$ a so that the averaged energy converges within 1000 realizations to within a 10 meV threshold.

III. RESULTS AND DISCUSSION

We first consider the case in which the on-site disorder is small compared to the energy gap, $\delta E = 10$ meV. The density plot in Fig. 3(a) shows a very broad distribution of *e-h* energies and separations, with the energy of an electron-hole pair generally increasing as charges move farther apart. Figure 3(b) adds important detail to identifying the nature of the states by introducing a general sense of the state's direction through the dipole moment. The negative value of $\langle R_D \rangle$ indicates that configurations pointing from the acceptor to the donor contribute the most to a particular state of the system.

The densest region of both distributions corresponds to the inversion point, where an electron and a hole of the charge-transfer state trade places. In Fig. 3(a), this point is accompanied by an increase in the density of states around (5.5 a, 5 eV) and is followed by a sharp rise in energy for larger values of $\langle R \rangle$. We can interpret this as additional kinetic energy allowing an electron and a hole to traverse the lattice independently of the phases. However, it is also an artifact of using a system of a finite size. When a hole resides at the interface, the maximum distance an electron can separate is limited by the length of the acceptor region. As energy increases, more and more states that have achieved farthest possible separation accumulate increasing the density of states at $\langle R \rangle \approx 5.5$ a. Eventually, the *e-h* pair has enough energy to transfer to the state where a hole can move into the acceptor and an electron moves into the donor to maximize the distance between them. While this computational artifact would be greatly reduced by the the simulation of a larger lattice, it is still important to consider since constrained acceptor regions do occur in the morphologically complex OPVs. Figure S2 of supplementary material shows density of states as a function of $\langle R \rangle$ and $\langle R_D \rangle$ to ensure that the regions of greatest density match.

Figures 4(a) and 4(b) show that the energy-separation and energy-dipole distributions become smoother as site energies of the lattice become more disordered. Increasing δE narrows the region above 1.5 eV and pushes the corresponding CT states toward greater electron-hole separations and smaller dipole sizes. In Sec. II B, we discussed that each eigenstate of our model Hamiltonian combines energetic contributions from different types of configurations. Larger values of $\langle R \rangle$ imply greater contributions from all farther separated configurations, while, associated declining $\langle R_D \rangle$ indicates that a considerable

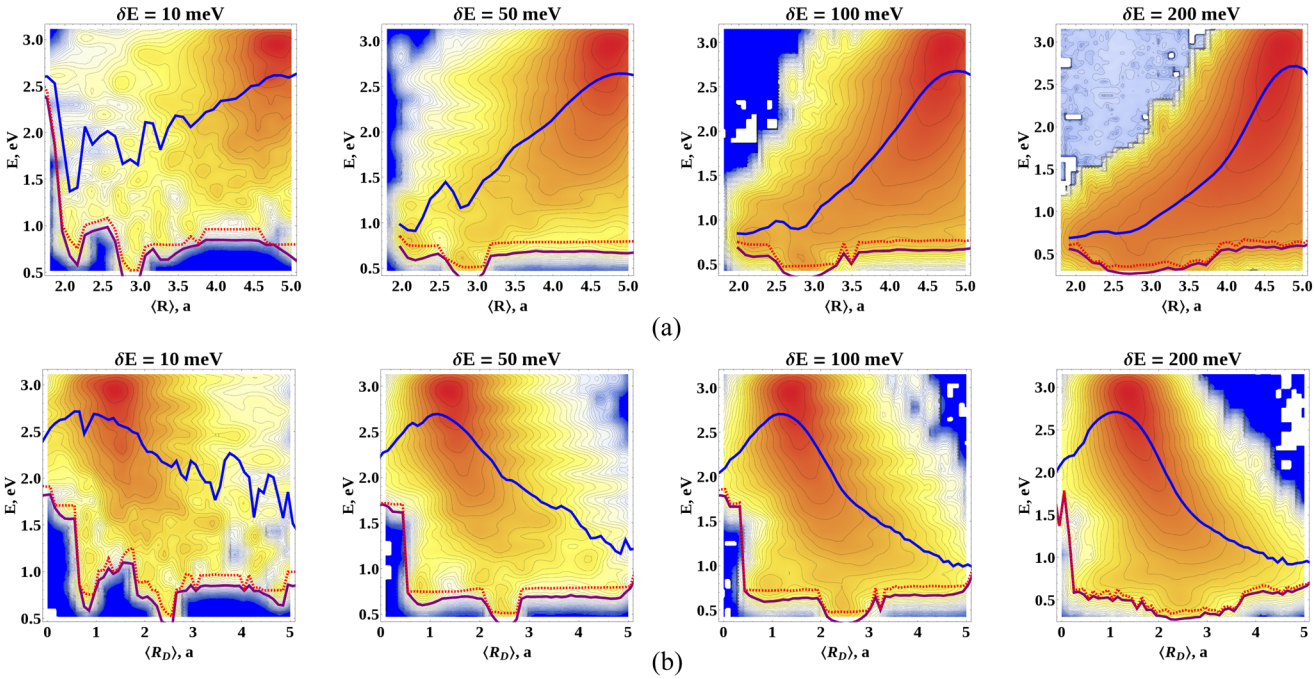

FIG. 4. Effect of site-energy disorder on the state energy distributions and thermodynamic and free energies of the system. Each panel shows charge distribution computed for specific values of site-energetic disorder δE. The color map is the same as in Fig. 3. The blue curve represents thermodynamic energy in the high temperature regime as a function of electron-hole separation, $\widetilde{E}$; the dashed red curve is thermodynamic energy at 298 K, $\langle E \rangle$; the purple curve is the free energy at 298 K, F White islands in each plot are plotting artifacts and do not carry any information.

fraction of these configurations are "flipped." At the same time, disorder broadens the lower region of both distributions and fills the gaps with new CT states, including states with higher values of both $\langle R \rangle$ and $\langle R_D \rangle$. Such states would have the most charge-transfer character since they are predominantly composed of configurations with a hole in the donor and an electron in the acceptor.

Plotting $\widetilde{E}(R)$ and $\langle E(R) \rangle$ over distributions shows how these curves highlight trends and features of the higher and lower energy regions, respectively. Physically, $\widetilde{E}$ describes the thermodynamic energy of the system in the high temperature limit ($\beta \to 0$). Since all states in this regime are equally probable, parts of the distribution with the greater density of states have greater influence on the value of $\widetilde{E}$. On the other hand, at $T = 298$ K, $e^{-\beta E_1} \gg e^{-\beta E_j}$, where $E_j > 1.5$ eV and lowest energy states determine $\langle E \rangle$ and F at every interval. Even though these states are not as numerous, their contribution, when thermally weighted, is far greater and any shift in their energy will be immediately reflected on the graphs. Despite $\widetilde{E}(R)$ requiring temperatures that would be impractical for OPVs, we believe that both energy curves play very important roles in the charge separation. While the system cannot place an exciton in a more energetic CT state at $T = 298$ K, the photons illuminating the device have a sufficient amount of energy (for visible light, $h\nu = 1.7$–3.0 eV) to realize any of the possible states of the system. After a photoexcitation, however, an electron-hole pair finds itself in the system equilibrated at 298 K, where F describes the energies of most probable states. Therefore, if the exciton does not dissociate into free charge carriers fast enough, it will relax to a lower CT state on the F curve and follow that path toward the polaron state. Based on the characteristics described above, we argue that the graphs of high temperature thermodynamic energy ($\widetilde{E}$) and 298 K free energy (F) curves correspond to the two experimentally observed mechanisms of charge separation: the direct ultra-fast charge transfer and the slower charge dissociation mediated by intermediate CT states.[21]

There is currently a lack of consensus regarding which pathway contributes the most to device performance. Investigations carried by Provencher *et al.* indicate that "hot" excitons can become charge carriers right away without the relaxation and lead to very high quantum efficiencies, while the effectiveness of electron transfer through the lower states heavily depends on the type of the blend used and the morphology of the device.[22] Savoie *et al.* showed that the rapid charge dissociation of the "hot" exciton is facilitated by the high density of acceptor states.[23] On the other hand, Vandewal *et al.* observed that the internal quantum efficiency in various photovoltaic blends is independent of whether the initial excited state is CT_1 (the lowest charge-transfer state) or any higher lying CT state. Measurements indicate that the very energetic states contribute little to the generation of free charges because they relax within the CT manifold before they can achieve greater separations.[24]

A proper statistical treatment allows us to recover both dissociation paths. While it has been suggested that the actual dissociation is a non-equilibrium process,[25] we do not look into the dynamics of individual charge transfers, but consider two thermodynamic regimes that are available to the excitons before and after relaxation. Ultra-fast "hot" electron-hole pairs can hop along the high energy curve without dissipating much energy, whilst the "cold" excitons travel along the equilibrated post-relaxation path.

We combine the associated energy curves for different values of δE in Fig. 5 to analyze the effect of increasing disorder on "hot" and "cold" excitons in greater detail. Variations in site-energies remove fluctuations from the average energy curve, $\widetilde{E}(\langle R\rangle)$, but steepen its gradient, increasing the overall energy needed to move an electron and a hole apart from 1 eV to 2 eV.

A. "Hot" exciton paths

In Fig. 5(b), the average energy for 1 a $< \langle R_D\rangle <$ 2 a corresponds to the densest region of the CT state distribution and does not change with disorder because additional lower energy states do not provide enough leverage. However, new states that appear below 1.5 eV do reduce $\widetilde{E}(\langle R_D\rangle)$ for other values of $\langle R_D\rangle$. Increased δE produces deeper minimum for $\langle R_D\rangle < 1$ a, but removes any fluctuations from the energy curve for $\langle R_D\rangle > 2$ a implying that greater disorder makes it harder for more energetic excitons to separate from each other, but once they are over the barrier, the energy path becomes unobstructed and steep, strongly favoring farther dissociation of an electron-hole pair.

The effect of disorder on "hot" excitons therefore is not straightforward. On one hand, the initial energy needed for the charges to separate increases at least two-fold with increasing δE, but on the other hand in the low disorder case, an *e-h* pair encounters a path with many energy barriers, especially at greater values of $\langle R_D\rangle$. To overcome these obstacles, an exciton will either have to dissociate through other states that are not on $\widetilde{E}(\langle R_D\rangle)$ or tunnel through the barriers to farther-separated states, in both cases decreasing the probability of the dissociation.

The average energy as the function of the absolute electron-hole separation, $\widetilde{E}(\langle R\rangle)$, [Fig. 5(a)] also shows that an electron and a hole can separate to greater distances in the high temperature regime; however, the mismatch between $\widetilde{E}(\langle R\rangle)$ and $\widetilde{E}(\langle R_D\rangle)$ and the associated densities of states at large values of $\langle R\rangle$ and $\langle R_D\rangle$ suggests that only a fraction of the states actually represents far-separated or long-range charge transfer states. As mentioned earlier, all possible electron-hole configurations contribute to the wavefunction of each state and as the energy of the exciton increases, so does the intraphase and flipped CT contributions. If we consider the entire distribution from Fig. 3, we can see "hot" excitons that dissociate into free charge carriers but never reach electrodes as the hole and the electron are in the opposite phases.

In previous studies, long-range CT (LCT) states have been associated with "hot" excitons;[26] however, our simulations show that since "hot" and "cold" paths are just different thermodynamic regimes, these states are available to low energy electron-hole pairs as well. In fact, as disorder increases, the region of the energy-dipole distribution composed of these states ($\langle R_D\rangle > 4$ a) narrows toward lower energy values.

B. "Cold" exciton paths

Free energy curves represent "cold" dissociation through lowest energy states. Our calculations of $F(\langle R\rangle)$ and $F(\langle R_D\rangle)$ for different values of δE reveal important aspects of the electron-hole separation, inaccessible to point-charge approximations. The energetic offset between donor and acceptor site energies divides all configurations into four types based on the location of an electron and a hole with respect to the interface (donor or acceptor intraphase CT, CT, and flipped CT states). We can characterize each eigenstate in the same way since in our model, the configurations that contribute the most to a particular state define its energy and separation. For example, states with 2.1 a $< \langle R\rangle <$ 2.7 a and 0.9 a $< \langle R_D\rangle <$ 1.9 a are predominantly composed of configurations with similar small separations. Among these configurations, the number of electron-hole CTs is significantly less than the number of intraphase configurations with the same separation. Therefore, states that fall into these intervals of $\langle R\rangle$ and $\langle R_D\rangle$ can also be classified as intraphase and the lowest energy electron-pairs dissociate as charges would if they were in a single material phase.

As an electron and a hole move farther apart, the eigenstates they occupy become more influenced by farther-separated charge-transfer configurations. Due to the energetic offset, ΔE, CT configurations have lower energy then donor intraphase configurations of the same electron-hole distance. Consequently, once the character of an exciton changes from intraphase to charge-transfer, it begins to follow a new lower free energy path. Both intraphase and charge-transfer segments of the free energy curves are essentially energetically shifted Coulombic potentials, and transfer of an exciton from the more to the less energetic path produces the minimum we see at $\langle R\rangle$ = 2.9 a and $\langle R_D\rangle$ = 2.4 a.

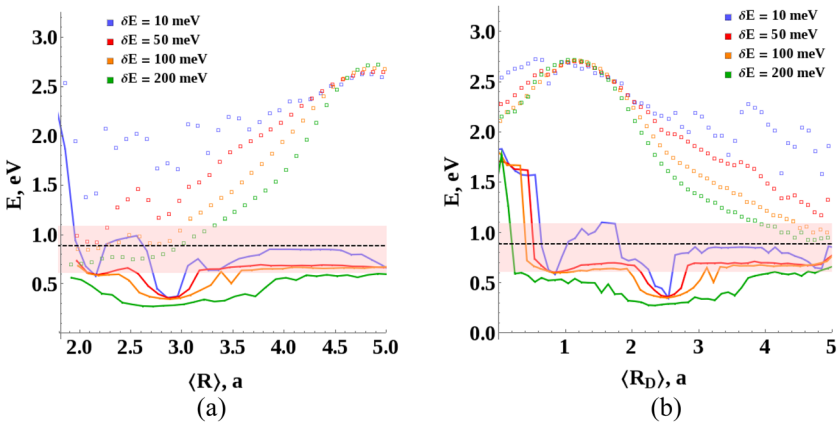

FIG. 5. Average (points) and free energy (solid) curves at different values of site-energy disorder δE. Shaded pink region represents the range of experimental values for open-circuit voltage with the average indicated by the dashed black line.

Figures 5(a) and 5(b) show that increasing site energy disorder significantly lowers the free energy, reducing Coulombic barriers in both segments of the curves and widening the minimum. Greater δE therefore has a mixed effect on the dissociation. While it reduces the attractive force between an electron and a hole, it also increases the size of the potential trap for CT states.

Overall similar shape and behavior of free energy curves, $F(\langle R\rangle)$ and $F(\langle R_D\rangle)$ indicate that the major contribution to these states comes from configurations with positive dipole moments. We explain this prevalence of the dipole orientation in the lower energy states by the presence of an internal potential difference, V_{OC}, which drives charges apart. In the Introduction of this paper, we talk about the equality of the free energy and the open-circuit voltage of the device (qV_{OC} for correct units.) The pink region of Fig. 5 corresponds to the range of experimental values of the open-circuit voltage obtained from different types of OPVs with disorder ranging from 60 to 104 meV.[10] We can see that F curves for $\delta E = 10$, 50, and 100 meV, apart from the energetic minimum, agree with the experimental data very well. We believe this agreement to be a crucial result not only because it validates the importance of the lower CT dissociation pathway, but also because it establishes a strong connection between theoretical models and experimental findings. Looking at the results of our calculations from the perspective of a open circuit voltage, we note that too much disorder will negatively impact the device performance. While most of the barriers inhibiting charge transfer completely disappear, the free energy curves decrease below the experimental range, leading to the drop of V_{OC} and efficiency.

To better understand all aspects of disorder in OPVs, we perform simulations of systems where we randomly modify values of the hopping integral (δt) and site coordinates (δx, δy). We start with the same reference system as for the δE calculations. Figure 6(a) shows that fluctuations in the hopping parameter have little effect on the $\widetilde{E}(\langle R_D\rangle)$ because "hot" excitons have sufficient kinetic energy to traverse the lattice with ease regardless of the values of the hopping term. The effect of $\delta t = 0.05$ eV on free energy is similar to the changes associated with $\delta E = 150$–200 meV. While a greater increase in the hopping disorder should facilitate the movement of an electron and a hole through the lattice and there are a number of energetically low highly separated states, too much disorder significantly decreases the free energy and therefore the open-circuit voltage, leading to a poor device performance. In addition, larger values of the hopping disorder widen and shift the free energy minimum, creating unfavorable energy gradient.

Previous studies relate disorder in electronic parameters of the OPVs to structural fluctuations in materials,[27,28] which we model by introducing disorder (δx, δy) into the x and y coordinates of each site. [In our simulations $\delta x = \delta y$, and we will refer to (δx, δy) as δx.] Unlike δE and δt, these fluctuations directly affect Coulombic and exchange interactions that depend on site-to-site distances. Figure 6(b) shows that $\widetilde{E}$ does not respond to the increase in δx confirming that more energetic CT states or "hot" excitons can avoid Coulombic attraction after they overcome the initial barrier. However, for low laying states with the dipole size less the 3 a, greater values of δx significantly lower the free energy. We explain this by noting that electrostatic interactions are much more sensitive to changes in the charge-to-charge distances when charges are close to each other, therefore the disorder parameter δx has more influence at smaller $\langle R_D\rangle$. Since the second Coulombic barrier occurs farther and is reinforced by the interface energy, increasing disorder does not have any effect for $\delta x = 0.05$ a and $\delta x = 0.10$ a, and actually enlarges the barrier for $\delta x = 0.15$ a, opposing the efficient charge dissociation.

In addition to the study of disorder, we compute the energy curves for the systems with systematically increasing the driving force, represented as the energetic offset (Fig. 7). ΔE is closely related to the open-circuit voltage of an OPV and promotes charge dissociation at the interface helping an electron and a hole to overcome the electrostatic binding, but whether it has the desired effect is still debated.[29,30] Our calculations show that increasing the energetic offset between two phases clearly extends the maximum possible electron-hole separation from 1 a at no offset to more than 4 a at $\Delta E = 0.9$ eV. We also show that unlike other studied parameters, greater values of the offset can shift the entire distribution toward larger values of $\langle R_D\rangle$. In the absence of the energetic offset, increasing site-energy disorder lowers the Coulombic interaction and

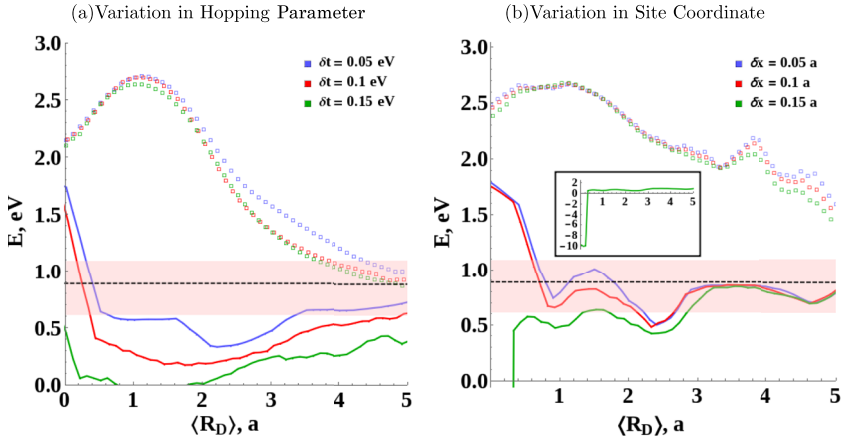

FIG. 6. The effect of hopping (a) and site coordinate (b) disorder on the electron-hole separation. Average and free energies are compared against experimental results. The inset in (b) shows full range of the free energy at 0.15 a of site coordinate disorder.

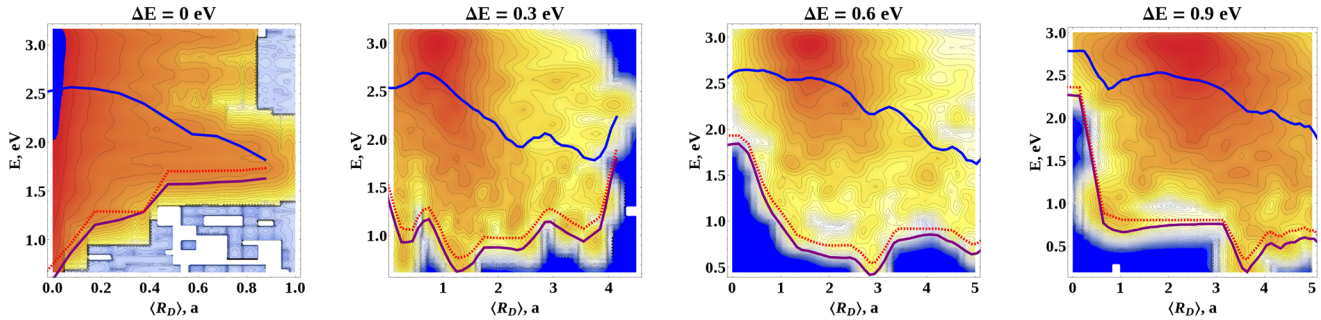

FIG. 7. Distributions of CT energies and dipole sizes for systems with increasing values of donor-acceptor energetic offset, ΔE. Thermodynamic (blue) and free (red) energy curves outline the most probably energetic paths for exciton dissociation.

free energy of the system but barely extends the overall charge separation, indicating that non-zero ΔE is necessary for the efficient charge dissociation to take place.

The downside of a large offset is manifested in the shift of the energetic minimum that can potentially trap an exciton at farther separations. As was mentioned earlier, the minimum occurs when the eigenstate of an electron-hole pair becomes predominantly a charge-transfer state. For intraphase electrons and holes, their Coulombic attraction is reduced by the energy difference between conduction and valence bands. The offset between the donor and the acceptor brings the conduction orbitals closer to the donor valence orbitals in terms of their energy. Therefore, even though δE favors the charge separation across the interface, an electron feels stronger electrostatic attraction toward the donor hole in a charge-transfer state.

IV. CONCLUSIONS

Recent studies have proposed that the dimensionality and disorder of organic photovoltaic materials ensure the successful charge separation despite strong Coulombic attraction between particles. We use the quantum mechanical lattice model[18,19] to explore the effect of disorder on charge dissociation and therefore on the performance of an OPV device. Our approach allows us to incorporate different forms of disorder by introducing fluctuations into the lattice parameters such as site energies, site-to-site transfer energies, and the site's physical location.

We compute eigenstates of the disordered system in the basis set of all electron-hole configurations of the corresponding lattice. The knowledge of each state's configurational composition allows us to compute their expected electron-hole separations and dipole sizes. The dipole size of an exciton represents the accurate distance between charges and the expected separation shows how much charge transfer character each state has. Matching state energies to the respective expected separations and dipole sizes produces two broad state distributions that can support numerous possible exciton dissociation paths, upholding the need for entropic considerations and free energy calculations.

The thermodynamic energy in the high temperature limit and the free energy at 298 K, computed as functions of the electron-hole distance, form the most probable energetic paths for excitons to dissociate through and resemble "hot" and "cold" dissociation mechanisms often discussed in the literature.[9,24,31–34] Thermodynamic energies of "hot" excitons show that while a lot of states have large expected separations, only handful actually correspond to far-separated CT states. Higher energies enable greater contributions of intraphase and flipped configurations that reduce the dipole size of a state and in many cases force electrons into the donor and holes into the acceptor regions, potentially removing them from the current generation.

Free energy outlines the "cold" dissociation path through the lowest energy CT states, however it turns out to be not as straightforward as expected from point charge estimations. Intraphase configurations with small electron-hole distances contributing the most to the states describing an electron and a hole are not far from each other, while long-range CT states are composed of highly separated charge-transfer configurations. The long-range states exhibit lower Coulombic energy due to the energetic offset between donor and acceptor regions. As a "cold" exciton dissociates along the free energy path, it first experiences the Coulombic attraction as an intraphase electron-pair. Once the charge transfer character of the states that make up the free energy curve reaches a certain point, an exciton's energy will drop to the one that describes dissociation of the charges separated by the interface. The transition results in a minimum in the free energy that can act as a trap for the dissociating excitons.

Increase in the site energy disorder has mixed effects on the "hot" and "cold" energy paths. Disorder increases the height of the initial energy barrier that highly energetic excitons need to overcome as they separate. At the same time, once the "hot" electron-hole pair is over the said barrier, greater disorder is beneficial for further separation as it makes the energy gradient steeper in the direction of separation and by removing any traps or additional barriers from the path. "Cold" excitons see the reduction in both intraphase and charge transfer Coulombic barriers as disorder increases due to the additional lower energy states. However, this decrease is accompanied by the widening of the energetic minimum that can act as a trap region for the charges. Transfer energy disorder has similar effect on the energy curves as the large values of site energy disorder, while disorder in site locations reduces only the first Coulombic energy peak of the free energy because the electrostatic attraction is more sensitive to the close range variations. Increasing energetic offset between donor and acceptor regions favors electron's initial separation across the interface;

however, it leads to stronger Coulombic attraction between the charges.

Apart from the minimum, the free energies for systems with 50, 100, and 150 meV of site-energy fluctuations are consistent with the values of open-circuit voltage (qV_{OC}) measured in OPV devices with similar amounts of disorder.[10,35] V_{OC} is one of the key parameters defining the performance of a solar cell and its connection allows us to establish a direct link between experimental and theoretical studies. Too much disorder of any kind greatly lowers the free energy and therefore reduces the open-circuit voltage and the efficiency of the device.

Computational cost-effectiveness and the general transferable set of parameters make our model a suitable tool to investigate the effects of molecular orientation, morphology, and dimensionality whose importance has been greatly emphasized in the literature.[6,29,36–39] A proper and self-consistent statistical treatment of the CT states leads to the correct understanding of the process of charge separation. By equating the free energy and the open-circuit voltage of the device, we establish a crucial connection between model predictions and experimental findings.

SUPPLEMENTARY MATERIAL

We provide a listing of all parameters used in our model in the supplementary material.

ACKNOWLEDGMENTS

The work at the University of Houston was funded in part by the National Science Foundation (Grant Nos. CHE-1664971 and MRI-1531814) and the Robert A. Welch Foundation (Grant No. E-1337).

[1] M. D. Chatzisideris, A. Laurent, G. C. Christoforidis, and F. C. Krebs, Appl. Energy **208**, 471 (2017).
[2] S. H. Park, A. Roy, S. Beaupre, S. Cho, N. Coates, J. S. Moon, D. Moses, M. Leclerc, K. Lee, and A. J. Heeger, Nat. Photonics **3**, 297 (2009).
[3] M. Scharber and N. Sariciftci, Prog. Polym. Sci. **38**, 1929 (2013), topical issue on Conductive Polymers.
[4] Z. He, B. Xiao, F. Liu, H. Wu, Y. Yang, S. Xiao, C. Wang, T. P. Russell, and Y. Cao, Nat. Photonics **9**, 174 (2015).
[5] S. Gélinas, A. Rao, A. Kumar, S. L. Smith, A. W. Chin, J. Clark, T. S. van der Poll, G. C. Bazan, and R. H. Friend, Science **343**, 512 (2014).
[6] A. C. Jakowetz, M. L. Böhm, J. Zhang, A. Sadhanala, S. Huettner, A. A. Bakulin, A. Rao, and R. H. Friend, J. Am. Chem. Soc. **138**, 11672 (2016).
[7] T. M. Clarke and J. R. Durrant, Chem. Rev. **110**, 6736 (2010).
[8] B. A. Gregg, J. Phys. Chem. Lett. **2**, 3013 (2011).
[9] S. N. Hood and I. Kassal, J. Phys. Chem. Lett. **7**, 4495 (2016).
[10] T. M. Burke, S. Sweetnam, K. Vandewal, and M. D. McGehee, Adv. Energy Mater. **5**, 1500123 (2015).
[11] S. Karabunarliev and E. R. Bittner, J. Phys. Chem. B **108**, 10219 (2004).
[12] E. R. Bittner and K. Stoyan, Int. J. Quantum Chem. **95**, 521 (2003).
[13] E. R. Bittner, S. Karabunarliev, and A. Ye, J. Chem. Phys. **122**, 034707 (2005).
[14] E. R. Bittner, J. Chem. Phys. **125**, 094909 (2006).
[15] E. R. Bittner, J. G. S. Ramon, and S. Karabunarliev, J. Chem. Phys. **122**, 214719 (2005).
[16] E. R. Bittner and C. Silva, Nat. Commun. **5**, 3119 (2014).
[17] E. R. Bittner, V. Lankevich, S. Gelinas, A. Rao, D. A. Ginger, and R. H. Friend, Phys. Chem. Chem. Phys. **16**, 20321 (2014).
[18] S. Karabunarliev and E. R. Bittner, J. Chem. Phys. **118**, 4291 (2003).
[19] S. Karabunarliev and E. R. Bittner, J. Chem. Phys. **119**, 3988 (2003).
[20] M. Tuckerman, *Statistical Mechanics: Theory and Molecular Simulation* (OUP, Oxford, 2010).
[21] C.-X. Sheng, T. Basel, B. Pandit, and Z. Vardeny, Org. Electron. **13**, 1031 (2012).
[22] F. Provencher, N. Berube, A. W. Parker, G. M. Greetham, M. Towrie, C. Hellmann, M. Cote, N. Stingelin, C. Silva, and S. C. Hayes, Nat. Commun. **5**, 4288 (2014).
[23] B. M. Savoie, A. Rao, A. A. Bakulin, S. Gelinas, B. Movaghar, R. H. Friend, T. J. Marks, and M. A. Ratner, J. Am. Chem. Soc. **136**, 2876 (2014).
[24] K. Vandewal, S. Albrecht, E. T. Hoke, K. R. Graham, J. Widmer, J. D. Douglas, M. Schubert, W. R. Mateker, J. T. Bloking, G. F. Burkhard, A. Sellinger, J. M. J. Fréchet, A. Amassian, M. K. Riede, M. D. McGehee, D. Neher, and A. Salleo, Nat. Mater. **13**, 63 (2014).
[25] L. Shi, C. K. Lee, and A. P. Willard, ACS Cent. Sci. **3**, 1262 (2017).
[26] M. Haibo and T. Alessandro, Adv. Mater. **26**, 6163 (2014).
[27] L. Simine and P. J. Rossky, J. Phys. Chem. Lett. **8**, 1752 (2017).
[28] H. Bässler and A. Köhler, Phys. Chem. Chem. Phys. **17**, 28451 (2015).
[29] N. E. Jackson, B. M. Savoie, T. J. Marks, L. X. Chen, and M. A. Ratner, J. Phys. Chem. Lett. **6**, 77 (2015).
[30] M. Scharber, D. Mühlbacher, M. Koppe, P. Denk, C. Waldauf, A. Heeger, and C. Brabec, Adv. Mater. **18**, 789 (2006).
[31] A. A. Bakulin, A. Rao, V. G. Pavelyev, P. H. M. van Loosdrecht, M. S. Pshenichnikov, D. Niedzialek, J. Cornil, D. Beljonne, and R. H. Friend, Science **335**, 1340 (2012).
[32] E. Vella, H. Li, P. Grégoire, S. M. Tuladhar, M. S. Vezie, S. Few, C. M. Bazán, J. Nelson, C. Silva-Acuña, and E. R. Bittner, Sci. Rep. **6**, 29437 (2016).
[33] R. D. Pensack and J. B. Asbury, J. Am. Chem. Soc. **131**, 15986 (2009).
[34] S. Athanasopoulos, S. Tscheuschner, H. Bässler, and A. Köhler, J. Phys. Chem. Lett. **8**, 2093 (2017).
[35] K. Vandewal, K. Tvingstedt, A. Gadisa, O. Inganäs, and J. V. Manca, Phys. Rev. B **81**, 125204 (2010).
[36] D. B. Sulas, K. Yao, J. J. Intemann, S. T. Williams, C.-Z. Li, C.-C. Chueh, J. J. Richards, Y. Xi, L. D. Pozzo, C. W. Schlenker, A. K.-Y. Jen, and D. S. Ginger, Chem. Mater. **27**, 6583 (2015).
[37] R. Noriega, J. Rivnay, K. Vandewal, F. P. V. Koch, N. Stingelin, P. Smith, M. F. Toney, and A. Salleo, Nat. Mater. **12**, 1038 (2013).
[38] J. R. Tumbleston, B. A. Collins, L. Yang, A. C. Stuart, E. Gann, W. Ma, W. You, and H. Ade, Nat. Photonics **8**, 385 (2014).
[39] A. C. Mayer, M. F. Toney, S. R. Scully, J. Rivnay, C. J. Brabec, M. Scharber, M. Koppe, M. Heeney, I. McCulloch, and M. D. McGehee, Adv. Funct. Mater. **19**, 1173 (2009).